Studying Altocumulus with Ice Virga Using Ground-Based Active and Passive Remote Sensors

Z. Wang
Goddard Earth Science and Technology Center
University of Maryland, Baltimore County
College Park, Maryland

Z. Wang, D. N. Whiteman, and B. B. Demoz
Mesoscale Atmospheric Processes Branch
National Aeronautics and Space Administration
Goddard Space Flight Center
Greenbelt, Maryland

K. Sassen
Geophysical Institute
University of Alaska
Fairbanks, Alaska

Introduction

Clouds not only play crucial roles in regulating the Earth-atmosphere system energy budget, but also the atmospheric hydrological cycle. The impact of a cloud system strongly depends on the cloud microphysical properties and its vertical extent (Stephens et al. 1990). Although clouds can contain only water droplets when >0°C and only ice crystals when < –40°C, between 0 and –40°C, clouds can be of ice, water, or mixed phase composition (Rauber and Tokay 1991; Cober et al. 2001). Cloud properties associated with different cloud phases within this temperature range are complicated and not well known. However, properly representing them in general circulation models (GCMs) is very important for climate simulation. Studies (Sun and Sjine 1994, Fowler et al. 1996) have also shown the treatment of mixed phase clouds in GCMs affect either their climate sensitivity or their mean climate impact. A better understanding of cloud physics within the mixed-phase regime is important for climate studies.

Mixed phase clouds have been mainly studied with in situ measurements (Heymsfield et al. 1991; Pinto 1998; Cober et al. 2001; Fleishauer et al. 2002), which provide detailed microphysical properties to understand the physical processes controlling mixed phase clouds. However, it is very expensive to accumulate large in situ measurements over long time periods and in different climate regions. Therefore, it is necessary to develop reliable ground-based and space-based remote sensing algorithms for their study. Recent developments and integrations of remote sensor technologies provide the possible means to achieve this challenging task. The U.S. Department of Energy (DOE) Atmospheric Radiation Measurement (ARM) Program Cloud and Radiation Testbed (CART) sites have been established in three climatic regimes: the Southern Great Plains (SGP), the Tropical Western Pacific (TWP), and the North Slope of Alaska (NSA) (Stokes and Schwartz 1994). The continuous high-quality

data streams from different passive and active remote sensors at these CART sites provide the opportunity to study mixed phase clouds in these dissimilar climate regimes. In this study, we begin our effort to develop algorithms to study a simple type of mixed phase cloud: Supercooled altocumulus with ice virga.

Instruments

Millimeter-Wavelength Cloud Radar (MMCR)

The MMCR is a zenith-pointing radar with 2 m diameter antenna that operates at 34.86 GHz (8.7-mm wavelength), and has a sensitivity of about -50 dBZe at 5.0 km altitude (Moran et al. 1998).

Micropulse Lidar (MPL)

The MPL is a compact eye-safe lidar that measures cloud base heights and aerosol profiles from the surface to about 20 km in the absence of strongly attenuating clouds (Spinhirne 1993). However, the low pulse energy limits its ability for high cloud measurements during daytime with high background signals. On the other hand, its unattended operation and neglable multiple scattering effects makes it to be a valuable system for cloud studies, especially at the TWP and NSA sites, where the MPL is the only currently available lidar system. Cloud layer transmittance can be calculated from lidar measurements when clear air returns above cloud top are available, permitting cloud layer optical depth to be estimated.

Microwave Radiometer (MWR)

The MWR receives nadir microwave radiation from the sky at 23.8 GHz and 31.4 GHz. Cloud liquid water in the atmosphere emits in a continuum that increases with frequency, dominating the 31.4 GHz observation, whereas water vapor dominates the 23.8 GHz channel. The water vapor and liquid water signals can, therefore, be separated by observations at these two frequencies (Hogg et al. 1983). Statistical retrieval methods are usually employed to derive water vapor path and liquid water path (LWP) from the total absorption. In current ARM data, the regression residual error or 'theoretical accuracy' of LWP is about 0.03 mm or 10 times the sensitivity or noise limit (0.003 mm) of the MWR. This detectable level limits MWR capability to measure LWP in many mid-level supercooled clouds.

Atmospheric Emitted Radiance Interferometer (AERI)

The "heart" of the AERI radiometer is a Fourier- transform infrared (IR) spectrometer, including the calibration blackbodies with temperature controllers. The AERI measures the absolute IR spectral radiance of the sky also in the nadir direction. The spectral measurement range of the instrument is 500 to 3300 cm^{-1} (20 to 3 μm) with a spectral resolution of 1.0 cm^{-1}.

Algorithm Description

Altocumulus cloud with ice virga can be generally regarded as two connected cloud layers where the top is the water-dominated source cloud and the bottom is an ice cloud, although it is also necessary to study ice within the water-dominated source cloud. In this section, we discuss details of the algorithms to retrieve the microphysical properties of ice virga and water-dominated source cloud through combined ground-based active and passive remote sensing.

Ice virga. We treat ice virga below the water-dominated source cloud as cirrus-like ice clouds and apply a previous lidar-radar algorithm (Wang and Sassen 2002) to derive the ice water content (IWC) and general effective size (D_{ge}) profiles. In the lidar-radar algorithm, IWC and D_{ge} are retrieved from the radar reflective factor (Z_e) and cloud extinction coefficient (σ) estimated from lidar measurements. The MMCR typically detects the relatively strong signals from ice virga because of their large particle sizes, despite their small concentrations. However, ice virga is usually optically thin, and we normally need to estimate σ of the virga from the backscattering coefficient by assuming an extinction-to-backscattering ratio (lidar ratio). Statistics of measured lidar ratios from the LIRAD method and Raman lidar indicate that values in cirrus clouds are most likely within the range of 15 to 20, and slightly depend on cloud temperature (Sassen and Comstock 2001). Therefore, the accuracy of σ estimated from the backscattering coefficient using a lidar ratio of 18 should be reasonable statistically.

Supercooled water-dominated source cloud. The basic properties of water cloud layers are LWP and cloud droplet effective radius (r_{eff}) because their radiative properties can be derived from these two basic parameters. However altocumulus clouds usually have small LWP values, which are often too small for current MWR to detect (Wang and Sassen 2001). Thus, it is best to rely on other instruments, such as AERI and lidar. Unlike stratus or stratocumulus clouds, which are often too optically thick for lidar to penetrate, supercooled altocumulus clouds can often be penetrated by lidar to measure cloud layer physical and optical depths and cloud optical properties. Although having small LWP, altocumulus clouds emit significant signals in the IR window region for AERI to generally detect. The general principles and basic retrieval steps to use AERI for cloud studies are discussed by Smith et al. (1993), and here we discuss an optimal approach to combine AERI and lidar to derive LWP and r_{eff} for altocumulus clouds.

The co-existence of these relative small and large imaginary indices within the IR window region (8-13 μm) results in an even larger difference in water droplet absorption capability and cloud layer IR emittance at different wavelengths, such that IR radiances within this region are widely used for cloud property retrieval (Strabala et al. 1994; Ackerman et al. 1995). The in situ measurements have indicated that water droplets have r_{eff} from about 4 up to 15 μm (Heymsfield et al. 1991; Fleishauer et al. 2002). Therefore observations within the IR window contain sensitive information for the study of droplet size according to Mie theory. Figure 1 presents cloud droplet extinction and absorption efficiencies as a function of sphere radius for the wavelengths listed in Table 1. It is clear that different wavelengths reach their peak extinction and absorption efficiencies at different droplet sizes, making IR window observations of water clouds promising.

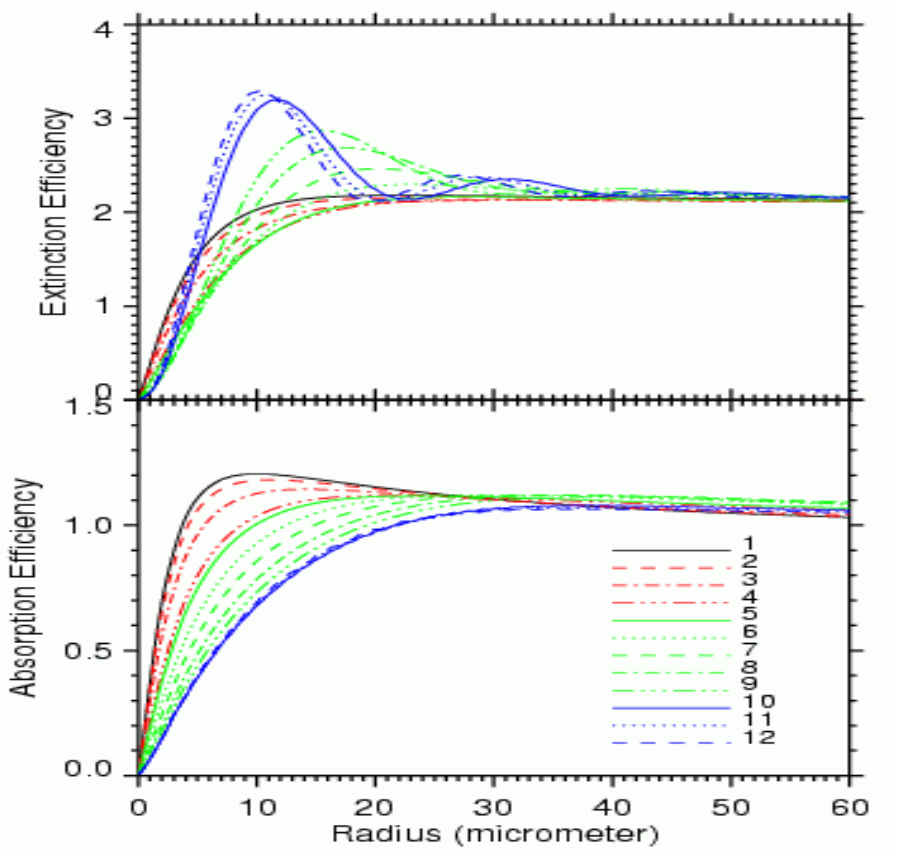

Figure 1. Water droplet extinction and absorption efficiencies as a function of water droplet radius for wavelengths listed in Table 1.

Table 1. Selected AERI Wavelengths for Altocumulus Cloud Retrieval

	Wavenumber (cm^{-1})	**Wavelength (μm)**
1	772	12.95
2	790	12.66
3	820	12.20
4	862	11.60
5	875	11.43
6	900	11.11
7	930	10.75
8	960	10.42
9	990	10.10
10	1090	9.17
11	1130	8.85
12	1160	8.62

To minimize the possible random errors, and to take advantage of information contained within different wavelengths and the high spectral resolution of the AERI, we select 12 low atmospheric absorption wavelengths between atmospheric absorption lines ranging from 772 to 1160 cm^{-1} (Table 1). Then we search for solutions of LWP and r_{eff} through minimizing the function F defined as:

$$F = \sum_{i=1}^{12} \left(\frac{I'(\lambda_i)}{I(\lambda_i)} - 1 \right)^2 , \quad (1)$$

where, $I(\lambda_i)$ and $I'(\lambda_i)$ are the measured and calculated downward radiances at wavelength λ_i, respectively. $I'(\lambda_i)$ is calculated using the discrete ordinate radiative transfer (DISORT) package (Stamnes et al. 1988) with inputs including water cloud optical properties parameterized as function of LWP and r_{eff}, and the molecular absorption optical depth profile is obtained from moderate-resolution atmospheric radiance and transmittance model.

The required cloud properties of each layer in the DISORT package are: cloud optical depth, single-scatter albedo (ω), and asymmetry factor (g) for phase functions calculated using the Henyey-Greenstein approximation. In the retrieval, the optical depth of the water-dominated layer is calculated with the LWP and cloud mass extinction coefficient (k), and k, ω, and g are parameterized as functions of LWP and r_{eff}. For the virga radiative properties, we use the parameterization developed by Fu et al. (1998) based on IWC and D_{ge}, which come from the lidar-radar algorithm.

One limitation using AERI downward radiance to study clouds is that cloud emissivity should be less than unity. Figure 2 presents emissivity as a function of LWP for two different r_{eff} values, which clearly shows that the slope of the emissivity to LWP relation decreases as LWP increases. To maintain good retrieval accuracy, it is better that the cloud has an emissivity less than 0.8, at least for the less absorbing wavelengths. Differences between Figure 2a and b suggest that the upper limit of LWP that we can retrieve is strongly dependent on r_{eff}, and we can at least retrieve LWP up to 30 g/m^2 for r_{eff} = 5.25 μm. Therefore, AERI can cover the lower end of LWP values that the MWR is unable to measure, and we will show this point again in following case studies.

The main error sources in the retrieval are measurement errors in radiances and cloud temperature, and the errors associated with a change of water vapor with time. The effect of temporal variations of water vapor can be partially corrected for with the total precipitable water measured by the MWR (Comstock and Sassen 2001) or temporal profiles measured by Raman lidar. The measurement errors in radiances can be divided into random error and systematic measurement errors, the latter due to instrument calibration and other factors. Simulations based on case studies discussed below indicate that ±1% systematic calibration error in all wavelengths causes about 3.1% and 2.4% mean error in LWP and r_{eff}, respectively. Random measurement errors are simulated with zero means and the standard deviations of 2 % of measured radiances, which can result in 2.4% and 5.0% error in LWP and r_{eff}, respectively. Similarly, ± 1°C cloud temperature error also results in 2.8% and 3.3% errors. Based on these simulations, we estimate uncertainties in retrieved LWP and r_{eff} is approximately <15%.

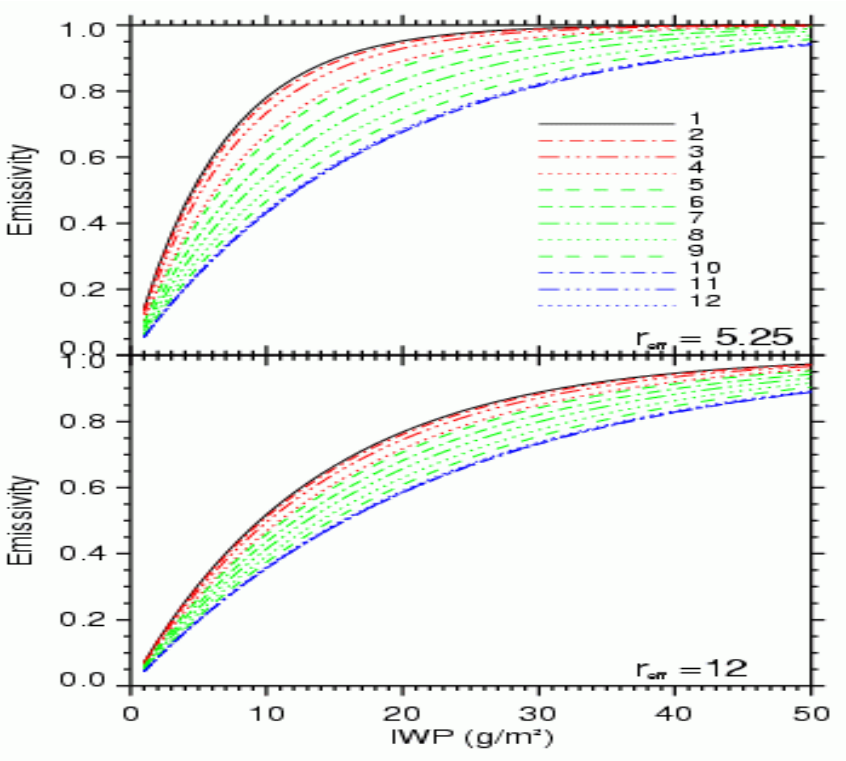

Figure 2. Emissivity of water clouds as a function of LWP for two different r_{eff} for wavelengths listed in Table 1.

There is a simple relationship between LWP and visible optical depth (τ):

$$\tau = \frac{3}{2\rho}\frac{LWP}{r_{eff}} \qquad (2)$$

where ρ is water density. If the cloud is optically thin (τ 3), τ can be derived from lidar measurements. With negligible multiple scattering effects, such as often with the MPL because of its narrow field of view, the lidar-derived τ can have good accuracy. Although combining τ with LWP derived from other measurements can also be used to derive r_{eff} from Eq. (2), unfortunately, current MWR designs cannot provide reliable low LWP values. Therefore, we use only lidar-derived τ as a closure test to examine the retrieval accuracy of LWP and r_{eff} here.

Case Studies

The case we examine is from the NSA CART site on January 18, 2000. At this site, it appears that altocumulus with ice virga happens more frequently than at the mid-latitude CART site, and can last for more than ten hours, as in the case we study here. During January 18, 2000, a precipitating altocumulus appeared at ~0500 Universal Time Coordinates (UTC) and gradually dissipated at the end of day when high clouds moved in. Figure 3a-c shows Z_e, mean Doppler velocity, and the logarithm of MPL

returned power between 0400 and 1200 UTC. The differences between the lidar and radar signals result from the different number concentrations and particle sizes in the water and ice clouds with respect to the different remote sensor wavelengths. The supercooled water dominated source cloud is indicated by the strong MPL signal and relatively weak Z_e due to a high concentration of small droplets. The black lines in Figure 3 represent the supercooled water-dominated cloud base determined from MPL measurements (Wang and Sassen 2001). It is clear that the ice virga below the source cloud is strong and stable. Relative humidity (RH), temperature, and potential temperature profiles from a radiosonde launched at 1831 UTC are presented in Figure 4. During this time, the cloud base descended to about 2 km from its initial ~3 km base height. The temperature profile shows that supercooled water clouds is at approximately -23°C and there is a more than 3°C temperature inversion at the cloud top, and the potential temperature profile indicates a moist stable layer below the inversion.

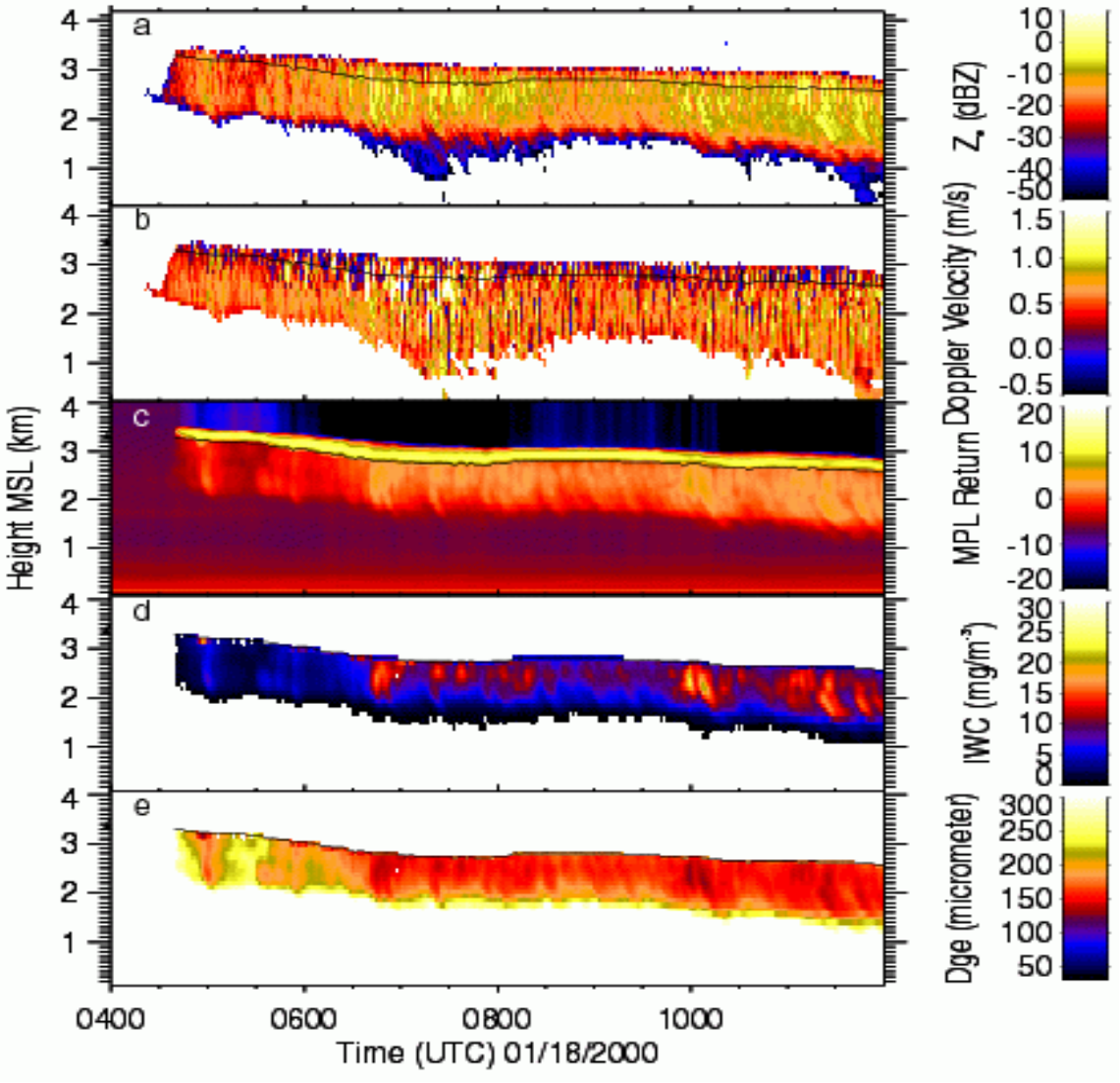

Figure 3. (a) Display of Z_e, (b) mean Doppler velocity, (c) MPL return power, (d) the retrieved IWC, and (d) D_{ge} of ice virga between 0400 and 1200 UTC on January 18, 2000, at the NSA CART site.

The retrieved IWC and D_{ge} profiles are displayed in Figure 3d and 3e, but ice virga in weak MPL signals is omitted because of possible relative large error in estimated extinction coefficients. The IWC image shows strong temporal variations and cellular structures. High IWC values generally correspond to relatively small D_{ge}, which suggests the strong variation in ice virga number concentration. Further understanding this variation in number concentration is important to better comprehend the generation of ice particles in the source cloud.

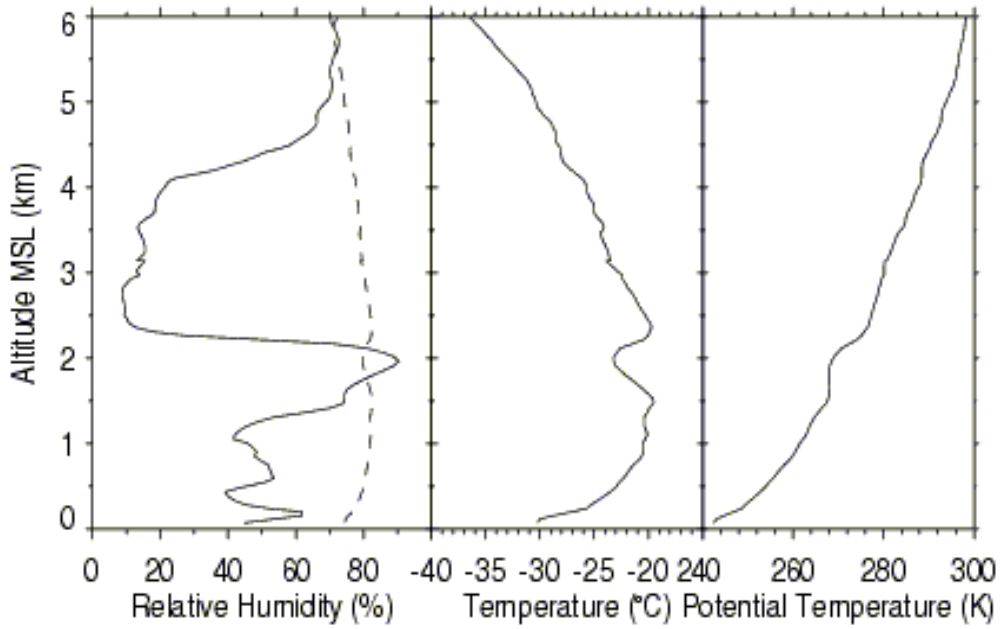

Figure 4. RH with respect to water, temperature, and potential temperature profiles from a radiosonde at 1831 UTC on January 18, 2000, where dashed line is ice saturation RH.

The retrieved LWP and r_{eff} for the supercooled water cloud component are presented in Figure 5a and 5b. The r_{eff} ranges from 4 to 7.5 μm as LWP changes from 2 to 12 g/m^2. For comparison, LWP values retrieved from the MWR measurements are shown in Figure 8a as the dashed line, and it suggests a clear-sky bias as large as 10 g/m^2 at 0430 UTC when no clouds are present. This bias is comparable to the maximum value of this altocumulus cloud. It is also clear that the pattern of LWP variations is also different, indicating large uncertainties for the low LWP values in MWR retrievals. An inhomogeneous nature of the precipitating altocumulus is revealed by the variations of LWP and r_{eff} as well as by the ice virga properties.

As mentioned above, τ can be estimated from lidar measurements and from retrieved LWP and r_{eff} data. A comparison of the results of the two methods (Figure 5c) can be used to validate the retrieved LWP and r_{eff}. The agreement is good except for two strongly attenuating periods from 0630 to 0800 and 1020 to 1150 UTC, which are clearly identified in the MPL power display in Figure 5c (note lower background above dense layer). The optical depth of the ice virga is given by the dashed line. Though it is only about one-tenth of the water layer optical depth, its contribution to the downwelling IR radiance is important for the retrieval of the water layer properties.

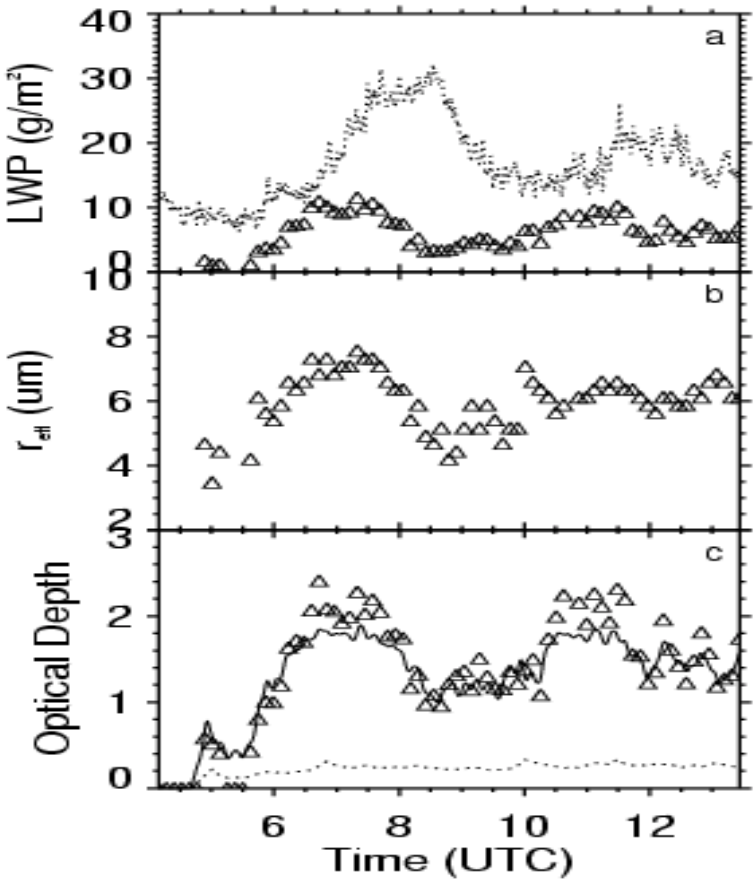

Figure 5. (a) The retrieved LWP and (b) r_{eff} for the supercooled water clouds on January 18, 2000, at the NSA CART site. In (a), LWP estimated from the MWR is given as dashed line. The comparison between visible optical depths for water dominated cloud layer derived from the MPL (solid line) and the LWP and r_{eff} (triangle symbols) is given in (c), and the optical depth of ice virga is shown as dashed line.

Summary

A combined active and passive remote sensing approach is presented for the study of supercooled liquid altocumulus cloud with ice virga. First, we treat the virga as a cirrus-like ice cloud, and apply a lidar-radar algorithm to retrieve IWC and D_{ge} profiles. Then an iterative approach is developed to retrieve supercooled water cloud properties by minimizing differences between observed IR radiances with the DISORT calculated radiances at 12 selected wavelengths. The inputs for the DISORT calculations include cloud temperature determined from radiosonde temperature profile and lidar/radar identified cloud height, a molecular absorption profile, and retrieved ice virga properties. A sound theoretical base and error analyses based on simulations indicate that this iterative approach provides reliable retrieval of LWP and layer mean r_{eff} for supercooled water clouds. One limitation of this approach is that it is only applicable to clouds with IR absorption optical depth less than 3.

This multiple remote sensor approach is applied to mixed-phase cloud case studies observed at the NSA and SGP CART sites. The results illustrate the capabilities of this approach to retrieve important microphysical properties needed to radiatively characterize this type of mixed phase cloud. The good agreement between visible optical depths derived from lidar measurement and estimated from LWP and r_{eff} provide a closure test for the accuracy of the mainly AERI based supercooled water cloud retrieval. Applying this analysis approach to larger CART datasets to better understand mixed-phase clouds and their possible differences in diverse climate regimes is an ongoing goal to improve cloud parameterization in GCMs.

Acknowledgement

This research has been funded by U.S. Department of Energy Grants DE-FG02-03ER63536 and DE-FG03-03ER63530 from the Atmospheric Radiation Measurement Program.

Corresponding Author

Zhien Wang, Zhien@agnes.gsfc.nasa.gov, (301) 614-6827

References

Ackerman, S. A., W. L. Smith, A. D. Collard, X. L. Ma, H. E. Revercomb, and R. O. Knuteson, 1995: Cirrus cloud properties derived from high spectral resolution infrared spectrometry during FIRE II. Part II: Aircraft HIS results. *J. Atmos. Sci.*, **52**, 4246-4263.

Cober, S. G., G. A. Isaac, A. V. Korolev, and J. W. Strapp, 2001: Assessing cloud phase condition conditions. *J. Appl. Meteor.*, **40**, 1967-1983.

Comstock, J. M., and K. Sassen, 2001: Retrieval of cirrus cloud radiative and backscattering properties using combined lidar and infrared radiometer (LIRAD*)* measurements. *J. Ocean. Atmos. Tech*., **18**, 1658-1673.

Fleishauer, R. P., V. E. Larson, and T. H. Vonder Haar, 2002: Observed microphysical structure of midlevel, mixed-phase clouds. *J. Atmos. Sci.*, **59**, 1779-1804.

Fowler, L. D., D. A. Randall, and S. A. Rutledge,1996: Liquid and ice cloud microphysics in the CSU general circulation model. Part I: Model description and simulated microphysical processes. *J. Climate*, **9**, 489-529.

Fu, Q., P. Yang, and W. B. Sun, 1998: An accurate parameterization of the infrared radiative properties of cirrus clouds for climate models. *J. Climate*, **11**, 2223-2237.

Heymsfield, A. J., L. M. Milosevich, A. Slingo, K. Sassen, and D. O'C. Starr, 1991: An observational and theoretical study of highly supercooled altocumulus. *J. Atmos. Sci.*, **48,** 923-945.

Hogg, D. C., M. T. Decker, F. O. Duirard, K. B. Earnshaw, D. A. Merritt, K. P. Moranm, W. B. Sweezy, R. G. Strauch, E. R. Westwater, and C. G. Little, 1983: A steerable dual-channel microwave radiometer for measurement of water and liquid in the troposphere. *J. Climate Appl. Meteor.,* **22**, 789-806.

Moran, K. P., B. E. Martner, M. J. Post, R. A. Kropfli, D. C. Welsh, and Widener, 1998: An unattended cloud-profiling radar for use in climate research. *Bull. Amer. Meteor. Soc.*, **79**, 443-455.

Pinto, J. O., 1998: Autumnal mixed-phase cloudy boundary layers in the Arctic. *J. Atmos. Sci.*, **55**, 2016-2037.

Rauber, R. M., and A. Tokay, 1991: An explanation for the existence of supercooled water at the tops of cold clouds. *J. Atmos. Sci.*, **48**, 1005-1023.

Sassen, K., and J. M. Comstock, 2001: A mid-latitude cirrus cloud climatology from the Facility for Atmospheric Remote Sensing: III. Radiative properties. *J. Atmos. Sci.,* **58**, 2113-2127.

Smith, W. L., X. L. Ma, S. A. Ackerman, H. E. Revercomb, and R. O. Knuteson, 1993: Remote sensing cloud properties from high spectral resolution infrared observations. *J. Atmos. Sci.*, **50**, 1708-1720.

Spinhirne, J. D., 1993: Micro Pulse Lidar. *IEEE Trans. Geosci. Remote Sensing*, **31**, 48- 55.

Stamnes, K., S. -C. Tasy, W. Wiscombe, and K. Jayaweera, 1988: A numerically stable algorithm for discrete-ordinate-method radiative transfer in multiple scattering and emitting layered media. *Appl. Opt.*, **27**, 2502-2509.

Stokes, G. M., and S. E. Schwartz, 1994: The Atmospheric Radiation Measurement (ARM) Program: Programmatic background and design of the cloud and radiation testbed. *Bull. Amer. Meteor. Soc.,* **75**, 1201-1221.

Stephens, G. L., S. Tsay, P. W. Stackhouse, and P. J. Flatau, 1990: The relevance of the microphysical and radiative properties of cirrus clouds to climate and climatic feedback. *J. Atmos. Sci.*, **47**, 1742-1753.

Strabala, K. I., S. A. Ackerman, and W. P. Menzel, 1994: Cloud properties inferred from 8-12 μm data. *J. Appl. Meteor.,* **33**, 212-229.

Sun, Z., and K. P. Sjine, 1994: Studies of the radiative properties of ice and mixed-phase clouds. *Quart. J. Roy. Meteor, Soc*., **120**, 111-137.

Wang, Z., and K. Sassen, 2001: Cloud type and macrophysical property retrieval using multiple remote sensors. *J. Appl. Meteor.,* **40**, 1665-1682.

Wang, Z. and K. Sassen, 2002: Cirrus cloud microphysical property retrieval using lidar and radar measurements: I algorithm description and comparison with in situ data. *J. Appl. Meteor.*, **41**, 218-22.